Available online at www.sciencedirect.com
ScienceDirect
Polymer 49 (2008) 1831–1840
polymer
www.elsevier.com/locate/polymer

Carbon nanotube dispersion and exfoliation in polypropylene and structure and properties of the resulting composites

Geon-Woong Lee[1], Sudhakar Jagannathan, Han Gi Chae, Marilyn L. Minus, Satish Kumar*

School of Polymer, Textile and Fiber Engineering, Georgia Institute of Technology, Atlanta, GA 30332, United States

Received 21 January 2008; received in revised form 8 February 2008; accepted 16 February 2008
Available online 21 February 2008

Abstract

Nitric acid treated single and multi wall carbon nanotubes (SWNT and MWNT) have been dispersed in polypropylene using maleic anhydride grafted polypropylene (MA-*g*-PP) and butanol/xylene solvent mixture. SWNT exfoliation was characterized by Raman and UV–vis–NIR spectroscopies. Evidence for hydrogen bonding between maleic anhydride grafted polypropylene and nitric acid treated nanotubes was obtained using infrared spectroscopy. Polypropylene/carbon nanotube composites were melt-spun into fibers. Dynamic mechanical studies show that for fibers containing 0.1 wt% SWNT, storage modulus increased by 5 GPa at −140 °C and by about 1 GPa at 100 °C, suggesting temperature dependent interfacial strength. The crystallization behavior has been monitored using differential scanning calorimetry and optical microscopy. Control fibers exhibited 27% shrinkage at 160 °C, while the shrinkage in the composite fibers was less than 5%. Fibers heat-treated to 170 °C show very narrow polypropylene melting peak (peak width about 1 °C).

Keywords: Polypropylene; Carbon nanotubes; Dispersion

1. Introduction

Carbon nanotubes (CNT) can be dispersed in polymers in melt or in solution. Good dispersion has been reported in melt for polar polymers such as poly(methyl methacrylate) (PMMA) [1–4] and polycarbonate (PC) [5–8], and in solution for polyacrylonitrile (PAN) [9–11] and poly(vinyl alcohol) (PVA) [12–14]. CNT dispersion in non-polar polymers such as polypropylene during melt processing has yielded mixed results. For example, larger diameter (50–10 nm) vapor grown carbon nanofibers can be well dispersed in polypropylene melt [15–17], while single wall carbon nanotubes (SWNT) were not as well dispersed [18]. Techniques such as end-group functionalization [19–21], use of ionic surfactants [22], shear mixing [23,24] and plasma coating [25] have been used to improve dispersion and exfoliation of nanotubes in polymers. Polypropylene compatibility with fillers has been improved by matrix modification by grafting it with reactive moieties, such as acrylic acid, acrylic esters, and maleic anhydride [26–28]. Improvement in thermal and electrical properties of polypropylene/nanotube composites has been reported [2,15,23,29,30]. In this paper we report a method to disperse and exfoliate CNTs in polypropylene by a combined solution and melt processing approach as well as the structure and properties of the resulting composites.

2. Experimental

As-received 100 mg SWNTs (~35% metal impurity) or MWNTs (~2.5% metal impurity) were sonicated in 100 mL of 7 and 6 M nitric acid, respectively, for 1 h using a Branson bath sonicator 3510R-MT (100 W, 42 kHz) maintained at 25–30 °C. The sonicated dispersion was refluxed at 100 °C for 1 h. The resulting suspension was repeatedly washed in distilled water and filtered. The filtered nanotubes were dried at room temperature for one day. The resulting bulky nanotube

* Corresponding author. Tel.: +1 404 894 2490; fax: +1 404 894 8780.
E-mail address: satish.kumar@gatech.edu (S. Kumar).
[1] Present address: Korea Electrotechnology Research Institute, Korea.

0032-3861/$ - see front matter © 2008 Elsevier Ltd. All rights reserved.
doi:10.1016/j.polymer.2008.02.029

mat contained 80–85 wt% water as determined by thermogravimetric analysis (TGA) (TA Instruments, TGA 2950). This acid treated nanotube water mixture was dispersed and sonicated in butanol (150 mL) for 2 h.

Maleic anhydride grafted polypropylene (MA-*g*-PP) (900 mg) (Epolene E-43 from Eastman Chemical Co.; $M_w \sim 9100$ and $M_n \sim 3900$ g/mole, acid number of 45) was dissolved in 150 mL xylene at 100 °C. The acid treated CNT/butanol dispersion is then added drop by drop to the MA-*g*-PP/xylene solution. This solution was further stirred for 30 min at 100 °C while allowing partial solvent evaporation, and subsequently vacuum dried in an oven maintained at 85 °C for 24 h to obtain the MA-*g*-PP/CNT master batch. The weight concentration of nanotubes in the master batch was determined by thermogravimetric analysis.

Polypropylene (Formolene 5101M from Formosa Plastics Co., melt flow index of 8.0 g/min at 230 °C) was then blended with PP-*g*-MA/CNT master batch by melt mixing in internal mixer (CW Brabender Instruments Inc. – Model PL2000) at 220 °C, 50 rpm for 10 min. For melt blending, neat polypropylene was pulverized to powder in liquid nitrogen and dry blended with PP-*g*-MA/CNT master batch to improve mixing. The control sample was prepared by melt blending PP with PP-*g*-MA in 95:5 ratio. PP/PP-*g*-MA and PP/PP-*g*-MA/CNTs samples containing 0.1 and 1 wt% SWNT, and 1 wt% MWNT are referred to as PP, PP/SWNT (0.1), PP/SWNT (1), and PP/MWNT (1), respectively. In the current study, the effect of the addition of PP-*g*-MA on PP was not characterized as we only compare PP and PP/CNT samples containing comparable amounts of PP-*g*-MA. However, we note from the literature studies that the addition of PP-*g*-MA, results in lowering the polypropylene modulus [31,32].

The control and the composite fibers were melt-spun at 200 °C on a piston driven small scale spinning unit manufactured by Bradford Univ. Ltd., UK using 500 μm diameter single hole spinneret. Fibers were subsequently drawn to a draw ratio of 4.7 at 120 °C. Drawn fibers were tensile tested at a cross-head speed of 25.4 mm/min in Instron Tensile Tester (Model 1130) by attaching single filaments to cardboard tabs (25.4 mm gauge length). Thirty single fibers were tested for each sample. Dynamic mechanical analysis (DMA) was carried out on Rheometrics RSA III on 10 filaments at a gauge length of 25.4 mm in the temperature range of −150 to +150 °C at 1 Hz at a heating rate of 1 °C/min. Wide angle X-ray diffraction (WAXD) studies were performed on a Rigaku Micromax-002 WAXS/SAXS system operated at 45 kV and 0.66 mA equipped with a Rigaku R-axis IV++ 2-D detection system. The diffraction patterns were analyzed using Area Max V. 1.00 and MDI Jade 6.1 softwares. The crystal size was calculated using the Scherrer equation with $K = 0.9$. The polypropylene crystalline orientation is calculated using (040) and (110) planes and the Wilchinsky equation [33,34] using the previously described procedure [18].

Transmission electron microscopy (TEM) was performed on a Hitachi HF-2000 field emission gun TEM operated at 200 kV. TEM samples were prepared on lacey carbon coated 300 mesh copper grids (Electron Microscopy Sciences cat. # HC300-Cu). PP/SWNT (1) and PP/MWNT (1) bulk composite chunks were first boiled in xylene for about an hour in order to fragment the composite sample. These fragments were collected and further placed in xylene and boiled for 24 h. A drop of the suspension was placed on the TEM grid using a loop and dried in air. Crystallization of the bulk melt held at 220 °C for 5 min in a hot stage was observed on Leitz polarizing microscope when cooled to room temperature at 0.5 °C/min. For differential scanning calorimetry (DSC) (TA Instrument Q100) studies, samples were heated at 10 °C/min to 220 °C and cooled and re-heated at the same rate. The infrared spectra were recorded on an Equinox 55 (Bruker Optics) in KBr tablets. The fiber shrinkage was measured using Thermomechanical Analyzer (TMA) (Q400, TA instruments) by heating 10-filament bundle at 5 °C/min from room temperature to 170 °C at a stress of about 3.2 MPa. UV–vis–NIR spectra were recorded on Cary 5G (Varian) spectrometer using a thin film of nanotube composite. Raman spectroscopy was performed on Holoprobe Research 785 Raman Microscope using 785 nm incident laser wavelength with polarizer and analyzer parallel to each other. Scanning electron microscopy was carried out on Leo 1530 SEM.

3. Results and discussion

The saturation SWNT solubility in various organic solvents and solvent mixtures was measured using previously reported procedure [35,36]. Measured solubility for pristine (containing about 2 wt% catalyst, from Unidym Inc.) and acid treated SWNTs in various solvents and solvent mixtures are listed in Table 1. A broader selection of solvents can be used for dispersing the acid treated tubes as compared to the pristine as-purified and unpurified tubes. However, acid treatment does not improve the solubility significantly in solvents such as toluene and xylene. The acid treated tubes can be dispersed in a mixture of alcohol and xylene as shown in Fig. 1. Nanotube dispersion increased when butanol content increased from 0 to 11.2 mL (58.3 vol% of the total solvent), while keeping the amount of xylene constant at 8 mL.

The neat PP-*g*-MA spectrum (Fig. 2a) shows strong absorbance of polymaleic anhydride (1784 cm^{-1}) [37,38] and carboxylic acid C=O stretch (1715 cm^{-1}) [39] at self-hydrogen-bonded carboxyl groups (COOH). The

Table 1
Measured carbon nanotubes solubility in various solvents

Solubility[a] (mg/L)	As-purified SWNTs	Acid treated SWNTs
Toluene[c]	<1	<1
Xylene[c]	<1	<1
Ethanol[c]	<1	27
1-Butanol[c]	<1	25
Ethanol/xylene[b]	<1	17
Butanol/toluene[b]	<1	19
Butanol/xylene[b]	<1	20

[a] Sonication time was over 96 h and settling time was 12 h.
[b] Volume fraction (50/50) and solubility were measured using same procedure as in Ref. [36].
[c] From Ref. [36].

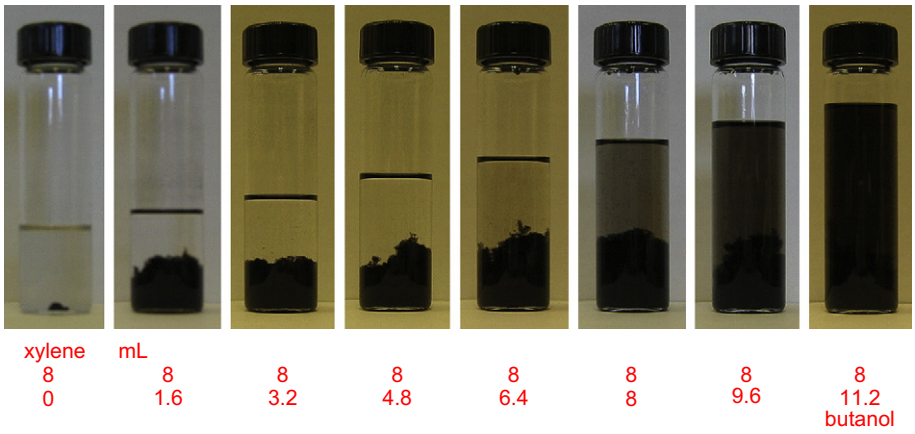

Fig. 1. Solubility of acid treated SWNTs in xylene/butanol mixture. Top and bottom rows indicate amount of xylene and butanol in milliliters, respectively. Acid treated SWNTs (1 mg) were dispersed in 8 mL xylene and sonicated for 30 min and the dispersion was allowed to settle for 2 h before taking a photograph. Subsequently, each time 1.6 mL butanol was added followed by sonication (30 min) and settling (2 h).

absorbance of polymaleic anhydride stretch (1784 cm^{-1} peak) was down shifted in PP/SWNT (0.1) composites and its relative intensity was reduced. This is due to hydrogen bond formation between polymaleic anhydride and PP/SWNT as schematically shown in Fig. 2b [37–40].

SEM images of the melt mixed bulk samples show good nanotube dispersion (Fig. 3). Fig. 4 shows fibril of about 15 nm diameter in the PP/SWNT (0.1) composite, and can be thought of as a SWNT bundle. After imaging Fig. 4a, sample was exposed to the electron beam for about 30 s, and imaged again at the same position (Fig. 4b). Fibril bending observed in Fig. 4b, suggests polymer coating on the nanotube. Due to electron beam irradiation, temperature increases and the polymer softens, resulting in the bending behavior. In the absence of polymer coating on the nanotube, 30 s electron beam exposure would have had no significant effect on its bending behavior. High resolution TEM images of PP/SWNT (1) and PP/MWNT (1) samples boiled in xylene for over 24 h show residual polymer on both SWNT and MWNTs (Fig. 5). The fact that all the polymer did not wash away in xylene even after boiling for 24 h suggest good polymer–CNT interaction.

It has been reported that Raman spectra can be used to probe the aggregation state of SWNTs [41]. PP-*g*-MA thin films were prepared with acid treated SWNTs using xylene/butanol mixture and the SWNT concentration in the films was about 0.25 and 5 wt%, respectively. Sample of 0.25 wt% was processed using xylene/butanol concentration below the solubility limit given in Table 1, while 5 wt% sample was processed above this concentration. Fig. 6 shows radial breathing mode spectra at laser excitation wavelength of 785 nm and film morphology of the two composite films as observed by SEM. In the figure, Raman spectra of the composites have also been compared to the spectrum of 100% carbon nanotube film. The spectral comparison in Fig. 6b reveals substantial diminution of the peak intensity at 267 cm^{-1} in the composite sample containing lower SWNT concentration (0.25 wt%), which is consistent with

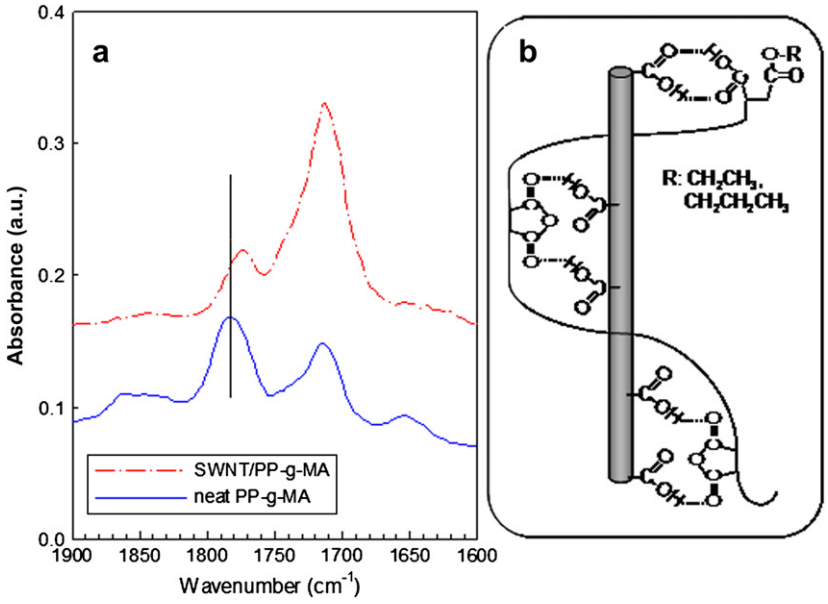

Fig. 2. (a) FTIR spectra of SWNT/PP-*g*-MA composite and neat PP-*g*-MA, and (b) the schematic diagram of hydrogen bonding between SWNT and PP-*g*-MA.

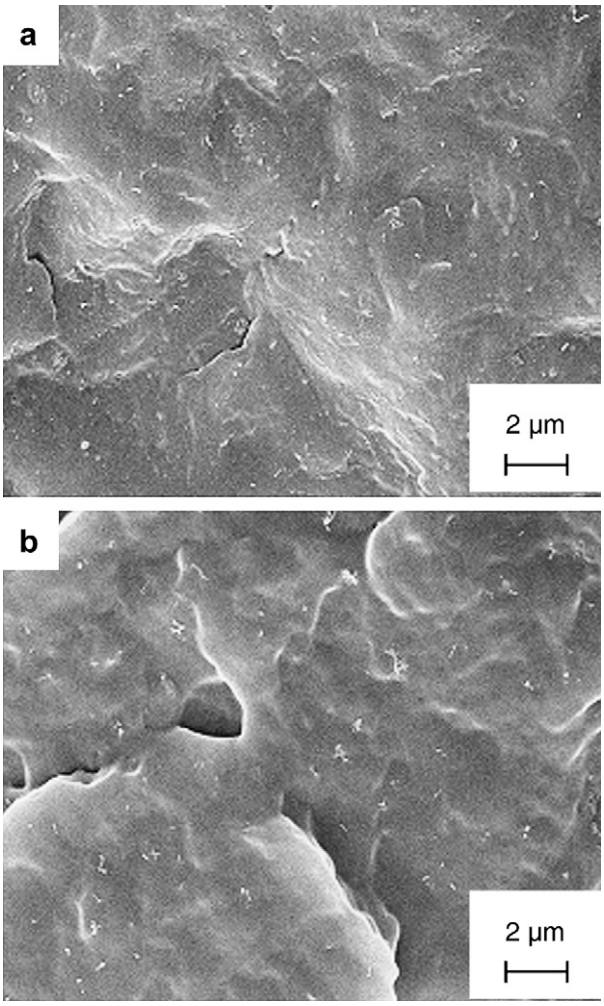

Fig. 3. Scanning electron micrographs of (a) PP/SWNT (1), and (b) PP/MWNT (1) melt mixed bulk samples.

significant SWNTs exfoliation, as discussed elsewhere [41]. By comparison, intensity of 267 cm^{-1} peak (Fig. 6a) is substantially higher, suggesting lower degree of exfoliation in 5 wt% SWNTs containing sample.

The UV–vis–NIR spectrum of composite film containing 0.25 wt% SWNT shows relatively well resolved van Hove transitions (Fig. 7) [42–44]. On the other hand, van Hove transitions for sample containing 5 wt% SWNTs are less well resolved. Based on the Raman, and UV–vis–NIR spectra, it can be concluded that the sample containing 0.25 wt% SWNT have a higher degree of exfoliation than 5 wt% SWNT containing samples. However, UV–vis–NIR spectrum does suggest some exfoliation even in 5 wt% SWNT containing samples. The UV–vis–NIR spectra of 0.25 wt% SWNT sample is blue shifted as compared to 5 wt% SWNT composite, suggesting interaction differences in the two cases. The shift of about 50 meV has also been reported for surfactant coated (such as sodium dodecyl sulfate – SDS) SWNTs [42–44]. Both the UV–vis–NIR and Raman spectroscopy provided evidence that when SWNT concentration below the saturation limit given in Table 1 is used then mostly exfoliated SWNTs can be obtained in the composite. Based on these

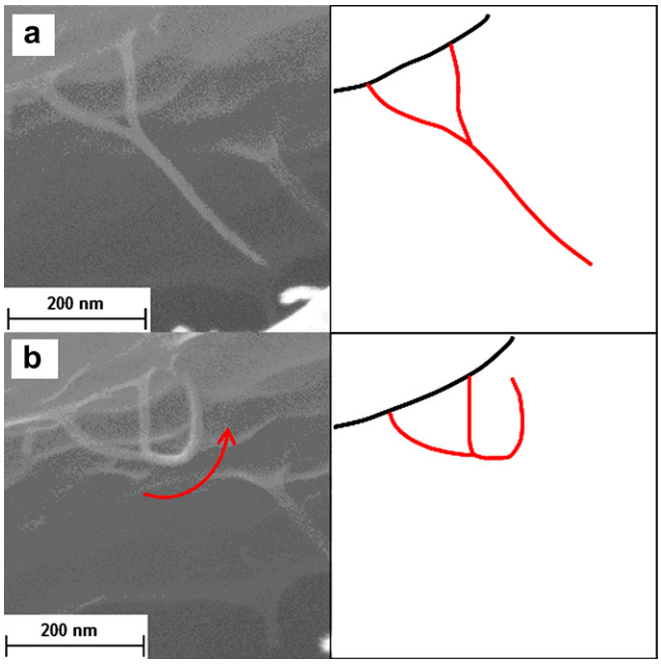

Fig. 4. SEM images of PP/SWNT composite: (a) before irradiation, and (b) after 30 s exposure to the 15 kV electron beam.

studies we conclude that exfoliated SWNTs are present in PAN/SWNT (0.1) and PAN/SWNT (1), though degree of exfoliation is expected to be higher at 0.1 wt% than at 1 wt%.

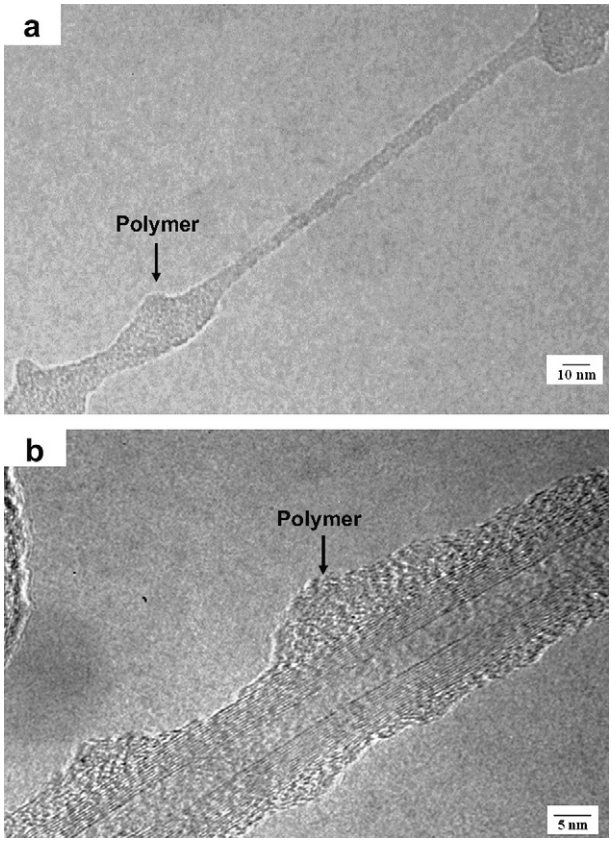

Fig. 5. High resolution transmission electron micrographs of (a) PP/SWNT (1) and (b) PP/MWNT (1) composite showing nanotubes covered by polymer. Both samples were boiled in xylene for 24 h before being examined in TEM.

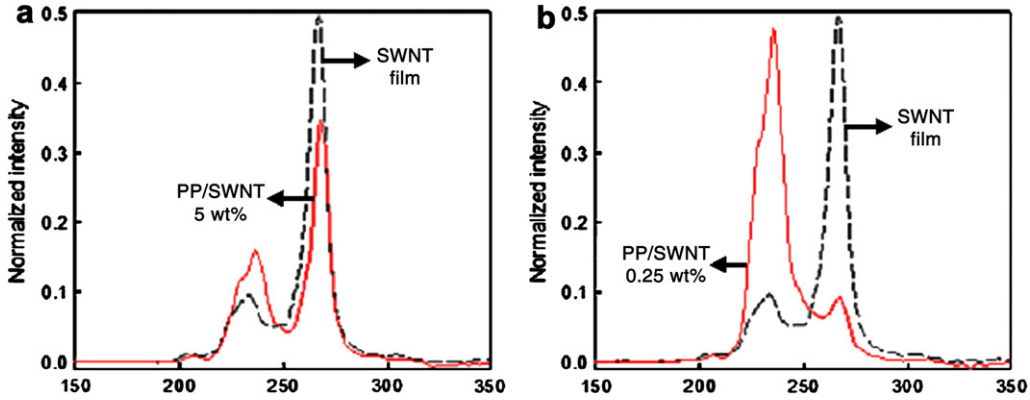

Fig. 6. Raman radial breathing mode (RBM) spectra normalized by tangential (G) band intensity of PP/SWNT. SWNT Raman spectra are given for comparison; (a) sample containing 5 wt% SWNTs, (b) partially exfoliated composites with 0.25 wt% SWNTs.

The SWNT orientation in the fiber can be determined from Raman tangential band ($\sim$1590 cm^{-1}) intensity, when spectra is collected as a function of polarization angle with respect to the fiber axis [10,45]. Raman tangential band intensities for PP/SWNT (1) and PP/SWNT (0.1) give Herman's orientation factors of 0.58 and 0.83, respectively. The tensile strength and modulus of PP/SWNT (0.1) fiber is about 25% higher than that of the control sample containing no nanotubes (Table 2). No further increase in modulus and strength was observed when SWNT concentration was increased to 1 wt%, in fact the properties were lower than that for the 0.1 wt% sample. This is attributed to insufficient nanotube exfoliation and relatively lower SWNT orientation in 1 wt% SWNT containing sample.

Dynamic mechanical analysis of polypropylene shows three relaxations at about −80 °C (α), 8 °C (β) and 100 °C (γ), respectively [46–48]. The γ peak is generally attributed to the relaxation of a few chain segments in the amorphous regions. The β-relaxation represents the glass transition, and α-relaxation is attributed to the lamellar slip and rotation in the crystalline phase [48]. In our control polypropylene fibers, tan δ plots (at a frequency of 1 Hz) show glass transition at about −7 °C, and at about 5 °C for the PAN/SWNT (1) (Fig. 8). The tan δ magnitude above the glass transition for all the composite samples is higher than that for the control polypropylene. Increase in tan δ peak was also observed for PMMA/carbon nanofiber [4] and PMMA/MWNT [1] composites. In PAN/SWNT, higher tan δ magnitude was also observed above the glass transition, with increasing SWNT content [11].

Storage moduli of various fibers as a function of temperature are compared in Fig. 9. The difference between the storage modulus of the composite (E'_{comp}) and control ($E'_{control}$) samples represents the contribution of nanotubes to the overall modulus (Fig. 10). For MWNT containing samples, $E'_{comp} - E'_{control}$ decreased from about 8 GPa at −140 °C to about 1 GPa at 100 °C, while the SWNT modulus contribution (both at 0.1 and 1 wt%)

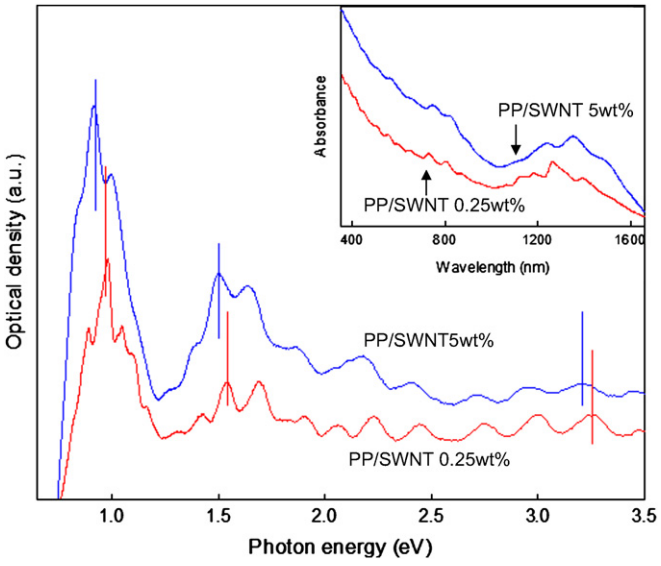

Fig. 7. Background subtracted UV–vis–NIR absorption spectra of PP/SWNT composite films. Inset shows the raw data.

Table 2
Tensile properties of various fibers

Sample	Tensile strength (GPa)	Elongation at break (%)	Tensile modulus (GPa)
PP	0.50 ± 0.05	35 ± 5	4.4 ± 0.3
PP/SWNT (0.1)	0.63 ± 0.06	35 ± 8	5.5 ± 0.3
PP/SWNT (1)	0.52 ± 0.06	28 ± 4	5.1 ± 0.4
PP/MWNT (1)	0.52 ± 0.06	30 ± 4	5.7 ± 0.5

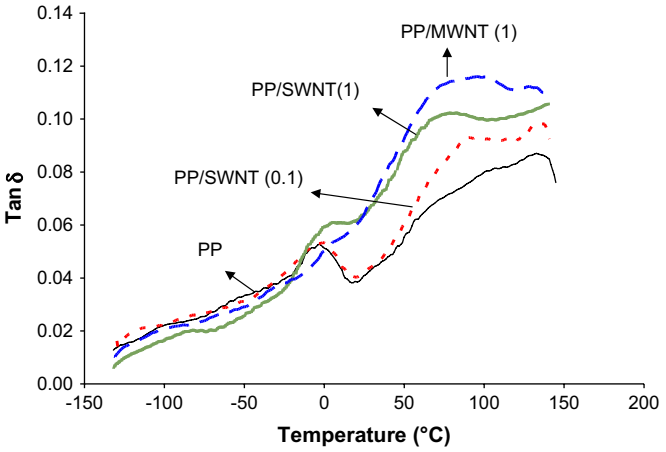

Fig. 8. Tan δ as a function of temperature for PP, PP/SWNT (0.1), PP/SWNT (1) and PP/MWNT (1) fibers tested at frequency of 1 Hz.

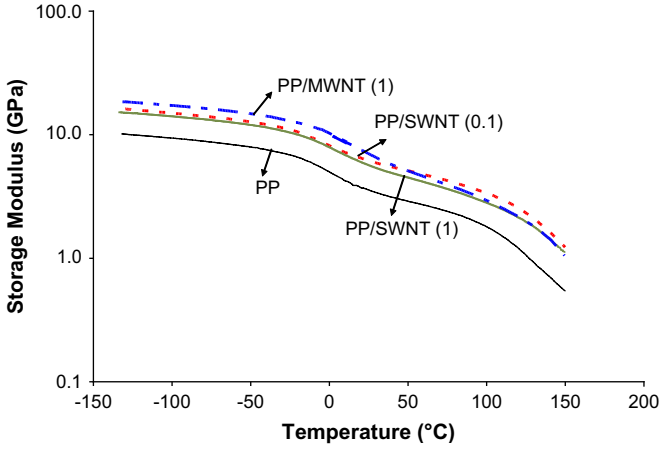

Fig. 9. Storage modulus of PP, PP/SWNT (0.1), PPSWNT (1) and PP/MWNT (1) fibers tested at a frequency of 1 Hz.

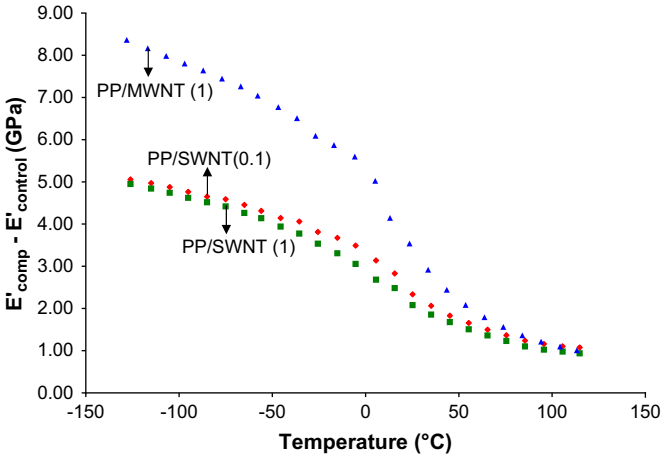

Fig. 10. Storage moduli difference between the composite and the control fibers as a function of temperature.

at −140 °C is about 5 and 1 GPa at 100 °C. Considering that the carbon nanotube modulus at 100 °C is more than 95% of its modulus value at −140 °C [49], the substantial drop in carbon nanotube contribution to the composite fiber modulus in this temperature range suggests highly temperature dependent nature of the load transfer efficiency and hence the interfacial strength in these composites. Modulus contribution of 5 GPa from 0.1 wt% nanotubes, even at −140 °C is noteworthy, and

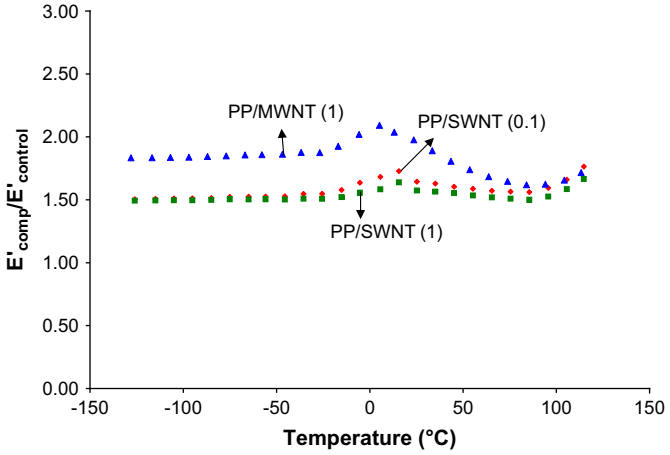

Fig. 11. Relative storage moduli ($E'_{Comp}/E'_{Control}$) for various composites as a function of temperature.

represents an effective SWNT modulus contribution of about 5 TPa. This modulus value is much higher than the SWNT modulus value of about 640 GPa, and may represent contributions from changes in polymer morphology due to the presence of SWNT. Change in interfacial strength or the load transfer efficiency between the polymer and the nanotubes as a function of temperature, at least partially may be due to the differences in the coefficient of thermal expansion of the two components – that is polymer and the nanotube [50–52]. Variation in load transfer efficiency as a function of temperature was also observed in PAN/SWNT composite fibers [9].

Ratio of composite to the control fiber storage moduli ($E'_{comp}/E'_{control}$) is higher at or near the glass transition temperature than above or below it (Fig. 11). Similar phenomenon for shear modulus ratio of composite to that of the control polymer was also observed in samples where reinforcing entities were spherical particles [50,53]. The jump in $E'_{comp}/E'_{control}$ near T_g was partially attributed to change in poisson's ratio of the polymer from about 0.35 below the glass transition temperature to about 0.50 near the glass transition temperature as well as to changes in the ratio of the modulus of the filler to that of the polymer in going through the glass transition [53].

DSC crystallization and melting data from first cooling and second heating cycles for bulk and fiber samples are given in Table 3. The percent crystallinity is calculated assuming that

Table 3
Non-isothermal crystallization and melting parameters for various samples for first cooling and second heating cycles

	Materials	Crystallization temperature T_c (°C)	FWHM[a] of crystallization peak, T_c (°C)	Crystallization enthalpy ΔH (J/g)	Melting temperature T_m (°C)	Melting enthalpy ΔH (J/g)	Crystallinity[b] (%)
Bulk	PP	114.8	7.1	103.5	167.2	101.9	49.2
	PP/SWNT (0.1)	123.1	4.5	102.6	166.2	104.8	50.6
	PP/SWNT (1)	126.3	3.7	100.3	165.3	101.2	48.9
	PP/MWNT (1)	120.8	4.4	103.3	164.0	102.9	49.7
Fiber	PP	116.8	6.8	118.7	165.1	114.3	55.2
	PP/SWNT (0.1)	121.1	5.0	114.3	165.2	113.1	54.7
	PP/SWNT (1)	126.7	3.1	115.1	163.9	114.7	55.4
	PP/MWNT (1)	122.4	3.4	110.3	163.7	107.8	52.1

[a] FWHM – full width at half maximum.
[b] Crystallinity calculated from enthalpy of melting.

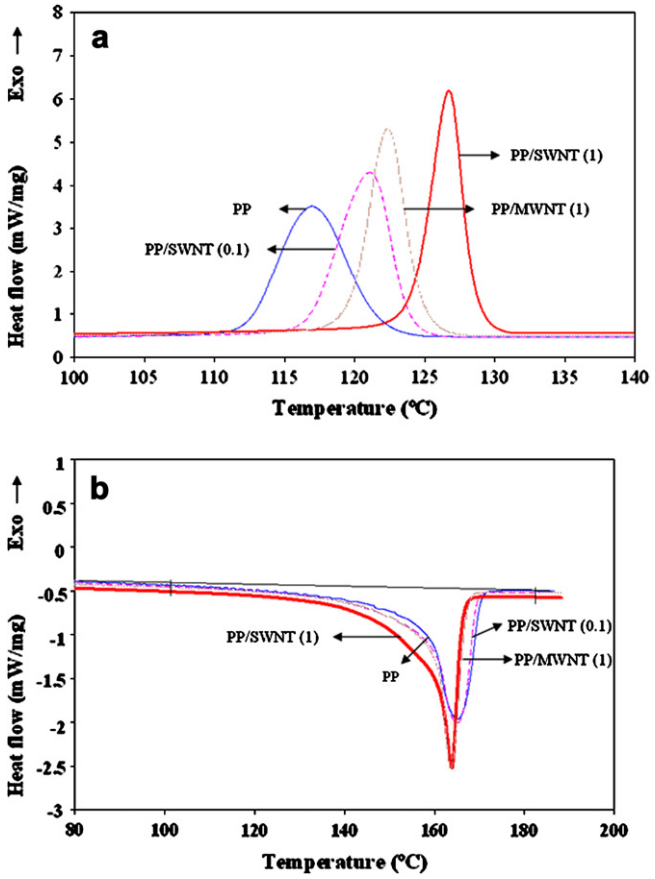

Fig. 12. DSC crystallization plots for various fibers: (a) first cooling cycle (b) second heating cycle. Plots for bulk samples not shown.

the enthalpy of melting of 100% crystalline polypropylene is 207 J/g [54,55]. The crystallization and melting peaks were integrated by fitting the baseline from 85–145 °C and 100–180 °C, respectively (Fig. 12). In both bulk and the fibers, the onset of crystallization occurs at higher temperature for the composites, suggesting that nanotubes act as nucleating agent. The crystallization and the melting peaks are narrower for the composite samples suggesting narrower crystal size distribution, in agreement with previous work [18]. The crystallization of bulk samples was also observed using Leitz polarizing optical microscope. For this purpose, bulk samples were melted at 220 °C and cooled at a rate of 0.5 °C/min. Fig. 13 shows that spherulite diameter decreased from about 400 μm in the control sample to about 20 μm in the composite, further confirming crystallization nucleation by carbon nanotubes.

Shrinkage at 160 °C in polypropylene fiber is about 27%, while in all the composite fibers, the shrinkage at this temperature is less than 5% (Fig. 14). This dramatic (80%) reduction in shrinkage, even at 0.1 wt% nanotubes, provides further evidence of interaction between CNT and polypropylene. In the absence of interaction, polypropylene in the composite would be as free to shrink as in the control sample. This interaction suggests that one should be able to disperse un-entangled nanotubes in polypropylene without functionalization or without the use of compatabilizers such as maleic anhydride grafted polypropylene used in the current study. This was recently demonstrated in MWNT/PP system, where MWNTs were first dispersed in dichlorobenzene [56]. Recent observation of polypropylene transcrystallinity on carbon nanotube, provided further evidence of PP–CNT interaction [57].

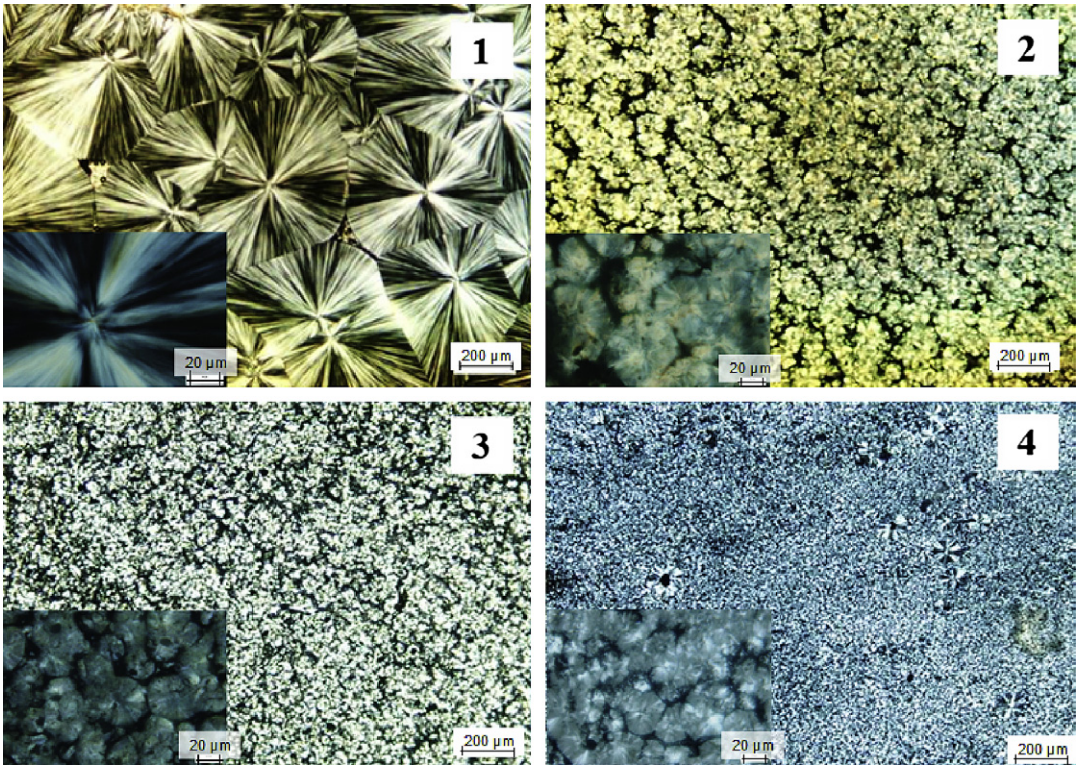

Fig. 13. Optical micrographs with cross-polarizers (1) PP, (2) PP/SWNT (0.1), (3) PP/SWNT (1), and (4) PP/MWNT (1) bulk samples.

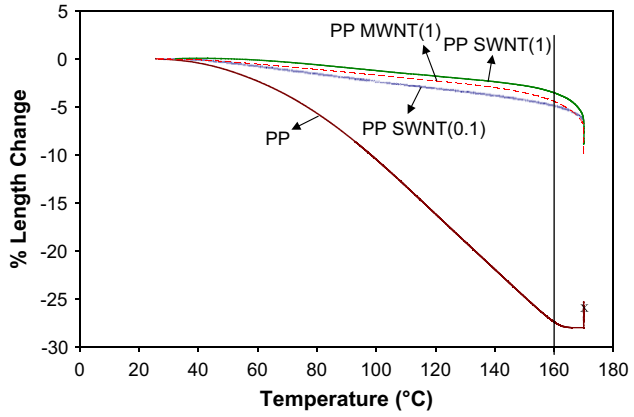

Fig. 14. Shrinkage behavior of various fibers at 3.2 MPa stress.

To further understand the shrinkage behavior, the drawn fibers were heated at 5 °C/min to 150, 160, and 170 °C (this is above the polymer melt temperature) in thermomechanical analyzer at a stress of 3.2 MPa, and held at the ultimate temperature for 5 min. Fibers were then cooled down to room temperature, and characterized by wide angle X-ray diffraction (Fig. 15). Polymer crystalline orientation increases for all the fibers, when they were heated up to 160 °C (Table 4). Considering that all fibers shrink even at 160 °C, increased crystalline orientation suggests that only the amorphous regions are responsible for the shrinkage at this temperature. At 170 °C, there is substantial decrease in polypropylene crystalline orientation in the control sample, while in composite fibers it decreases only marginally. At 160 °C, relatively small polymer crystals melt and re-crystallize. Tensile properties of the fibers heated to 160 °C under tension, were either comparable to or lower than that for the fibers without heat treatment. DSC melting behavior of the 160 °C sample, shows very sharp melting peak (peak width less than 1 °C) during first heating (Fig. 16). Such a sharp melting peak is typically not observed for polymers. However, the sharp melting peak is consistent with the large crystal size observed from X-ray. Broad melting peak is observed during the second heating, as expected. The crystal size increases on re-crystallization closer to the melting point [58,59]. The re-crystallized larger crystals show a melting point of 5–10 °C higher than the crystallized samples [60,61]. In our case fibers without heat treatment exhibited

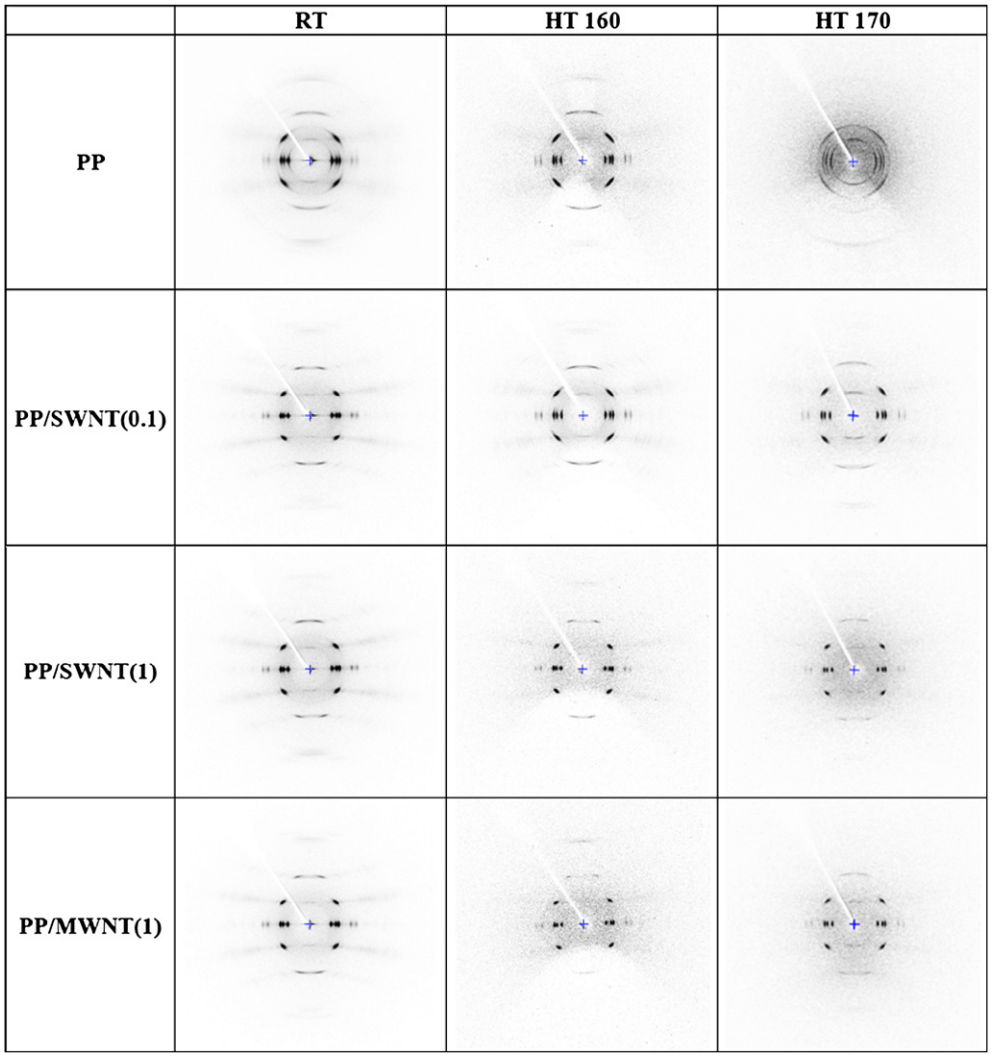

Fig. 15. WAXD diffraction patterns for various fibers.

Table 4
Crystal size, crystallinity, and Herman's orientation factor (f) for various fibers

	RT	160 °C	170 °C
Crystal size (nm) of (110) plane ($2\theta \sim 14°$)			
Control PP	10.9	26.6	36.0
PP/SWNT (0.1)	12.9	22.9	36.6
PP/SWNT (1)	13.4	18.8	29.2
PP/MWNT (1)	13.1	13.2	35.2
Crystallinity (%)[a]			
Control PP	69	76	80
PP/SWNT (0.1)	75	75	77
PP/SWNT (1)	73	78	75
PP/MWNT (1)	75	76	78
f_{pp}[b]			
Control PP	0.89	0.93	0.73
PP/SWNT (0.1)	0.92	0.94	0.88
PP/SWNT (1)	0.92	0.93	0.88
PP/MWNT (1)	0.93	0.94	0.86

[a] Crystallinity calculated from X-ray diffraction.
[b] f_{pp} is polypropylene c − axis orientation.

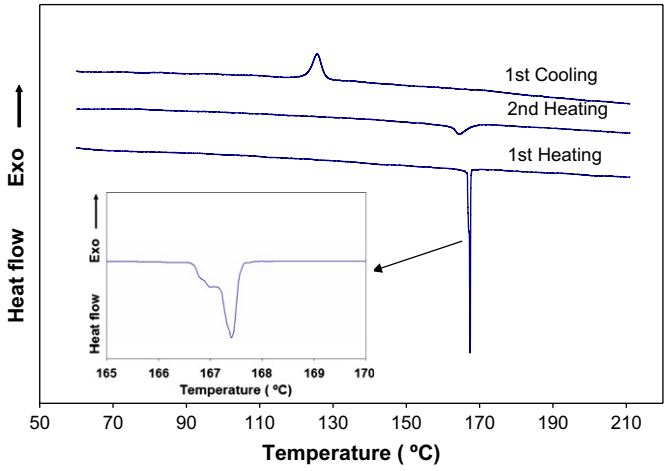

Fig. 16. DSC plot for PP/SWNT (0.1) fiber heated to 160 °C at 3.2 MPa stress. DSC studies were done without a stress or constrains. Other samples, including control PP fiber showed similar behavior. Inset shows that the sharp melting peak consists of two peaks.

a melting temperature of 164–165 °C, while the 160 °C heat-treated fibers exhibited the narrow melting peak above 167 °C (an increase of about 2 °C).

4. Conclusions

A method has been developed to disperse and exfoliate carbon nanotubes in polypropylene using a combined solution and melt processing approach. Dynamic mechanical analysis shows that 1 wt% well dispersed MWNT increase the storage modulus at −140 °C by 8 GPa and well dispersed and exfoliated 0.1 wt% SWNT increased it by 5 GPa at the same temperature. On the other hand the storage modulus increase in the two cases at 100 °C was only about 1 GPa. This suggests significant temperature dependent load transfer efficiency in the PP–CNT system. At 160 °C, there is 80% reduction in the thermal shrinkage of 0.1 wt% SWNT containing fiber as compared to the control polypropylene fiber. This reduction in the thermal shrinkage between PP and PP–CNT fibers provided evidence of interaction between the two entities. Direct evidence of interaction has also been observed from high resolution transmission electron microscopy.

Acknowledgement

This work was supported by the Office of Naval Research, Air Force Office of Scientific Research, and Post-doctoral Fellowship Program of the Korea Science & Engineering Foundation (KOSEF).

References

[1] Jin Z, Pramoda KP, Xu G, Goh SH. Chemical Physics Letters 2001;337(1–3):43–7.
[2] Park WK, Kim JH, Lee S-S, Kim J, Lee G-W, Park M. Macromolecular Research 2005;13:206–11.
[3] Russell E, Gorga REC. Journal of Polymer Science Part B: Polymer Physics 2004;42(14):2690–702.
[4] Zeng J, Saltysiak B, Johnson WS, Schiraldi DA, Kumar S. Composites Part B: Engineering 2004;35(2):173–8.
[5] Chen L, Pang X-J, Yu Z-L. Materials Science and Engineering: A 2007;457(1–2):287–91.
[6] Kim H-S, Park B-H, Kang M, Yoon J-S, Jin H-J. Key Engineering Materials 2006;326–328:1829–32.
[7] Fornes TD, Baur JW, Sabba Y, Thomas EL. Polymer 2006;47(5):1704–14.
[8] Potschke P, Brunig H, Janke A, Fischer D, Jehnichen D. Polymer 2005;46(23):10355–63.
[9] Chae HG, Minus ML, Kumar S. Polymer 2006;47(10):3494–504.
[10] Chae HG, Sreekumar TV, Uchida T, Kumar S. Polymer 2005;46(24):10925–35.
[11] Sreekumar TV, Liu T, Min BG, Guo H, Kumar S, Hauge RH, et al. Advanced Materials 2004;16(1):58–61.
[12] Minus ML, Chae HG, Kumar S. Polymer 2006;47(11):3705–10.
[13] Vigolo B, Penicaud A, Coulon C, Sauder C, Pailler R, Journet C, et al. Science 2000;290(5495):1331–4.
[14] Zhang X, Liu T, Sreekumar TV, Kumar S, Hu X, Smith K. Polymer 2004;45(26):8801–7.
[15] Hasan MM, Zhou Y, Jeelani S. Materials Letters 2007;61(4–5):1134–6.
[16] Kumar S, Doshi H, Srinivasarao M, Park JO, Schiraldi DA. Polymer 2002;43(5):1701–3.
[17] Sui G, Wei-Hong Z, Fuqua Mike A, Ulven CA. Macromolecular Chemistry and Physics 2007;208(17):1928–36.
[18] Bhattacharyya AR, Sreekumar TV, Liu T, Kumar S, Ericson LM, Hauge RH, et al. Polymer 2003;44(8):2373–7.
[19] McIntosh D, Khabashesku VN, Barrera EV. Chemistry of Materials 2006;18(19):4561–9.
[20] McIntosh D, Khabashesku VN, Barrera EV. Journal of Physical Chemistry C 2007;111(4):1592–600.
[21] Zhou Z, Wang S, Lu L, Zhang Y, Zhang Y. Journal of Polymer Science Part B: Polymer Physics 2007;45(13):1616–24.
[22] Vaisman L, Marom G, Wagner HD. Advanced Functional Materials 2006;16(3):357–63.
[23] Lopez Manchado MA, Valentini L, Biagiotti J, Kenny JM. Carbon 2005;43(7):1499–505.
[24] Xiao Y, Zhang X, Cao W, Wang K, Tan H, Zhang Q, et al. Journal of Applied Polymer Science 2007;104(3):1880–6.
[25] Donglu S, Jie L, Peng H, Wang LM, Feng X, Ling Y, et al. Applied Physics Letters 2003;83(25):5301–3.
[26] Kelarakis A, Yoon K, Sics I, Somani RH, Chen X, Hsiao BS, et al. Journal of Macromolecular Science Part B 2006;45(2):247–61.

[27] Ristolainen N, Vainio U, Paavola S, Torkkeli M, Serimaa R, Seppälä J. Journal of Polymer Science Part B: Polymer Physics 2005;43(14): 1892–903.
[28] Zhou X, Xie X, Zeng F, Li RK-Y, Mai Y-W. Key Engineering Materials 2006;312:223–8.
[29] Tjong SC, Liang GD, Bao SP. Scripta Materialia 2007;57(6):461–4.
[30] Jiang X, Bin Y, Kikyotani N, Matsuo M. Polymer Journal 2006;38:419–31.
[31] Kim DH, Fasulo PD, Rodgers WR, Paul DR. Polymer 2007;48(18): 5308–23.
[32] García-López D, Gobernado-Mitre I, Merino JC, Pastor JM. Polymer Bulletin 2007;59(5):667–76.
[33] Samuels R. Structured polymer properties. New York: Wiley; 1974. p. 28–41.
[34] Wilchinsky ZW. Journal of Applied Physics 1960;31(11):1969–72.
[35] Bahr JL, Mickelson ET, Bronikowski MJ, Smalley RE, Tour JM. Chemical Communications 2001;(2):193–4.
[36] Lee GW, Kumar S. Journal of Physical Chemistry B 2005;109(36): 17128–33.
[37] Karian HG. Handbook of polypropylene and polypropylene composites. 2nd ed. New York: Marcel Dekker; 2003. p. 44–56.
[38] Sclavons M, Carlier V, Roover BD, Franquinet P, Devaux J, Legras R. Journal of Applied Polymer Science 1996;62(8):1205–10.
[39] Garton A. Infrared spectroscopy of polymer blends, composites and surfaces, vol. 40. Munnich: Hanser Publishers; 1992. p. 181–195.
[40] Socrates G. Infrared and Raman characteristic group frequencies: tables and charts. 3rd ed. New York: Wiley; 2001. p. 117–30.
[41] Heller DA, Barone PW, Swanson JP, Mayrhofer RM, Strano MS. Journal of Physical Chemistry B 2004;108(22):6905–9.
[42] Hagen A, Hertel T. Nano Letters 2003;3(3):383–8.
[43] Moore VC, Strano MS, Haroz EH, Hauge RH, Smalley RE, Schmidt J, et al. Nano Letters 2003;3(10):1379–82.
[44] O'Connell MJ, Bachilo SM, Huffman CB, Moore VC, Strano MS, Haroz EH, et al. Science 2002;297(5581):593–6.
[45] Liu T, Kumar S. Chemical Physics Letters 2003;378(3-4):257–62.
[46] Amash A, Zugenmaier P. Journal of Applied Polymer Science 1997;63(9):1143–54.
[47] Liu X, Wu Q. Polymer 2001;42(25):10013–9.
[48] McCrum NG, Read BE, Williams G. Anelastic and dielectric effects in polymeric solids. London, New York: John Wiley and Sons; 1967.
[49] Lu JP. Physical Review Letters 1997;79(7):1297.
[50] Lee B-L, Nielsen LE. Journal of Polymer Science Part B: Polymer Physics Edition 1977;15(4):683–92.
[51] Putz Karl W, Mitchell CA, Krishnamoorti R, Green PF. Journal of Polymer Science Part B: Polymer Physics 2004;42(12):2286–93.
[52] Suhr J, Koratkar N, Keblinski P, Ajayan P. Nature Letters 2005;4: 134.
[53] Nielsen LE. Mechanical properties of polymers and composites, vol. 2. New York: Marcel Dekker; 1974.
[54] Velasco JI, De Saja JA, Martínez AB. Journal of Applied Polymer Science 1996;61(1):125–32.
[55] Wunderlich B. Thermal analysis. Boston: Academic Press; 1990. p. 418.
[56] Zhang S, Kumar S. Macromolecular Rapid Communications, in press doi:10.1002/marc.200700838.
[57] Zhang S, Minus ML, Zhu L, Wong C-P, Kumar S. Polymer 2008;49(5): 1356–64.
[58] Grasruck M, Strobl G. Macromolecules 2003;36(1):86–91.
[59] Strobl G. Progress in Polymer Science 2006;31(4):398–442.
[60] Avila-Orta CA, Medellín-Rodríguez FJ, Dávila-Rodríguez MV, Aguirre-Figueroa YA, Yoon K, Hsiao BS. Journal of Applied Polymer Science 2007;106(4):2640–7.
[61] Lima MFS, Vasconcellos MAZ, Samios D. Journal of Polymer Science Part B: Polymer Physics 2002;40(9):896–903.